



**HAL**  
open science

## Rheology of particulate rafts, films, and foams

Olivier Pitois, Florence Rouyer

► **To cite this version:**

Olivier Pitois, Florence Rouyer. Rheology of particulate rafts, films, and foams. *Current Opinion in Colloid & Interface Science*, 2019, 43, pp.125-137. <10.1016/j.cocis.2019.05.004>. <hal-02184505>

**HAL Id: hal-02184505**

**<https://enpc.hal.science/hal-02184505v1>**

Submitted on 28 Jun 2020

**HAL** is a multi-disciplinary open access archive for the deposit and dissemination of scientific research documents, whether they are published or not. The documents may come from teaching and research institutions in France or abroad, or from public or private research centers.

L'archive ouverte pluridisciplinaire **HAL**, est destinée au dépôt et à la diffusion de documents scientifiques de niveau recherche, publiés ou non, émanant des établissements d'enseignement et de recherche français ou étrangers, des laboratoires publics ou privés.



HAL Authorization

# Rheology of Particulate Rafts, Films and Foams

Olivier Pitois<sup>1</sup>, Florence Rouyer<sup>2</sup>

<sup>1</sup> Université Paris-Est, Laboratoire Navier, UMR 8205 CNRS, ENPC ParisTech, IFSTTAR,  
2 allée Kepler, 77 420 Champs-Sur-Marne, France

<sup>2</sup> Université Paris-Est, Laboratoire Navier, UMR 8205 CNRS, ENPC ParisTech, IFSTTAR,  
5 boulevard Descartes, 77 454 Champs-Sur-Marne, France

Liquid foam exhibits remarkable rheological behavior although it is made with simple fluids: it behaves like a solid at low shear stress but flows like a liquid above a critical shear stress. Such properties, that have been proved to be useful for many applications, are even enhanced by adding solid particles. Depending on their hydrophobicity and their size, the particles can have different geometrical configurations at the mesoscopic scale, i.e. at the air-liquid interfaces, in the films or the interstices between the bubbles. In this review, we present rheological studies performed on granular rafts and films, on spherical armored interfaces, on gas marbles and on aqueous foams laden with hydrophilic grains.

## Introduction

Since the pioneer works of Ramsden [1] and Pickering [2], it is known that the stability of oil-in-water emulsion can be drastically increased by using hydrophobic solid particles. For more than one century, many applications, from cosmetic, medical to food industries, have been developed on the principle that particles can adsorb at fluid interfaces to create armor-like protective layers, either for single droplets encapsulation purposes or for stabilizing assemblies of droplets or bubbles, i.e. as emulsions or foams respectively. Such a stabilization mechanism can be used to produce aerated materials without resorting to conventional carbon-based surfactants [3]. In this context, understanding the interfacial rheological behavior of armored interfaces is a major issue as it determines the physical properties of particle-laden systems, such as their deformation induced by external mechanical stress or their aging driven by intrinsic capillary stress [4,5]. Our purpose is to present studies performed on rheology of particle films and foams. Although foams and emulsions are very similar systems, gas bubbles are usually larger than liquid droplets, which allows for a wide range of particle sizes to be used in foam.

Last decade, many works [6–9] have clarified the influence of particle contact angle with respect to both dispersed and dispersing phases, i.e. oil/water or air/water: if the particles are not fully wetted by neither of the two fluid phases, they encapsulate the less wetting phase [6]. In Pickering concentrated emulsions and foams, drops and bubbles are separated by particulate films (cf. Figure 1-a). Those films can be made of two particle monolayers (cf. Figure 1-a top) or of one single particle monolayer (cf. Figure 1-a bottom). The former configuration is made of two particulate interfaces, one at each interface of the film. The later configuration can be obtained for intermediate particle wettability, which allows for the particles to be shared by both interfaces, i.e. to bridge the interfaces of two neighbor bubbles (or droplets) (cf. Figure 1-a bottom). Horozov et al. [8] showed that the bridging configuration is obtained mostly when repulsive forces exist between the particles. More recently, Timounay et al. [10] created free-standing particle films, by dipping and removing a frame through a particle raft (Figure 1-b), for which the particles can arrange in bilayer

or monolayer configurations depending on particle sizes and geometry of the frame. They showed that the particle configuration influences the bursting dynamics of armored liquid films. Within the bridging configuration, when a hole is created at the center of the armored film, it opens intermittently and the opening process can be stopped. For the other cases, constant retraction velocities are observed.

Stability and rheology of Pickering systems are expected to be closely related to the mechanical properties of the armored interfaces and films. Whereas appropriate surfactants can be chosen to prevent bubble coalescence events, long-term stability against both coalescence and ripening seems to be the strong feature of Pickering systems, provided that the particles are robustly attached to the interface and form a dense layer [11]. It is to say that applied shear has a catastrophic impact on Pickering foam stability, so a comprehensive study of their rheological behavior is still lacking. Some understanding can however be found with concentrated Pickering emulsions (although they are also subjected to coalescence [12]): they were found to exhibit both shear-thickening and shear-thinning behaviors depending on the particles used and the physicochemical parameters [13,14]. Shear-thinning can be understood by the shear-stress induced droplet elongation, which suggests that the particle armor is not strong enough. On the other hand, shear-thickening is reminiscent of rigid particle suspensions, which suggests that the particle armor can also behave like a solid shell.

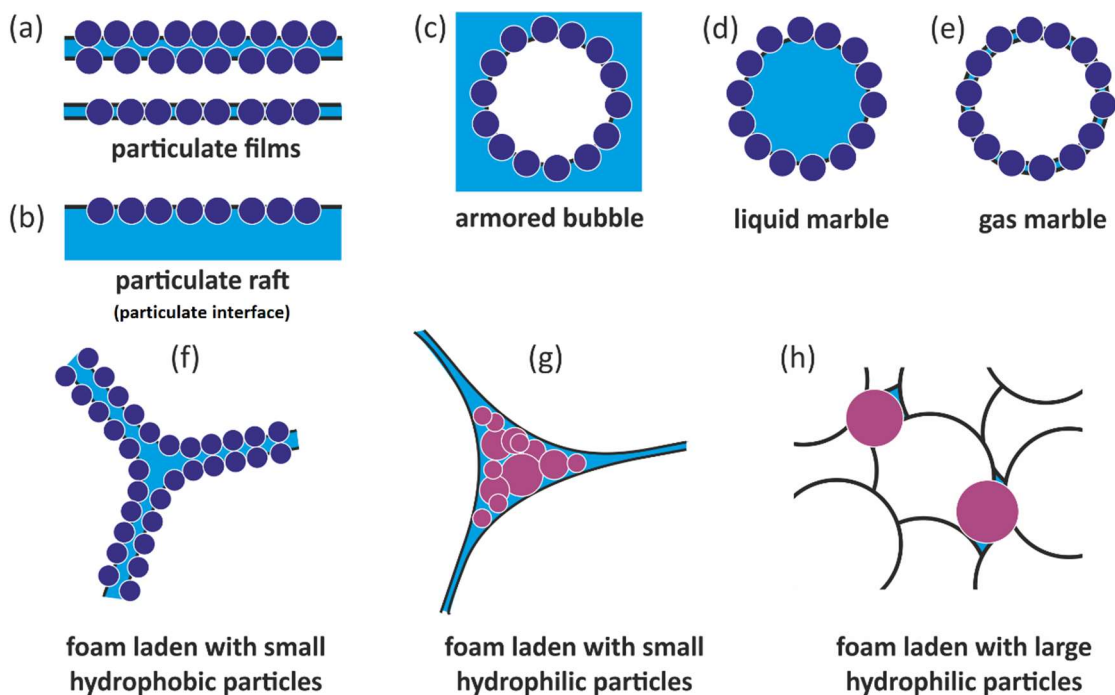


Figure 1 : Sketch of the different configurations for solid particles in liquid films and foams : (a) particles at the interfaces of a single liquid film, in the bilayer configuration (top) and monolayer, i.e. bridging, configuration (bottom); (b) solid particles on a single flat liquid interface, also called particulate raft; (c) solid particles at the curved interface of a bubble in liquid, also called armored bubble; (d) solid particles at the curved interface of a liquid droplet, also called liquid marble; (e) solid particles at the double-interface of a soap bubble, also called gas marble; (f) foam laden with small hydrophobic solid particles covering the interfaces; (g) foam laden with small hydrophilic solid particles that are dispersed in the continuous liquid phase ; (h) foams laden with large hydrophilic solid particles.

Hydrophilic particles do not attach to fluid interfaces but they can be trapped between the numerous interfaces that are formed within foams. Whereas large particles (i.e. larger than 1  $\mu\text{m}$ ) are rapidly squeezed out of contact areas between bubbles, smaller particles can form transient steric barriers against coalescence [15–17]. As far as we know, direct film rheology has never been performed on such films. On the other hand, study of foams made with hydrophilic colloidal particles suspension has shown that drainage can be significantly reduced, or even stopped, thanks to the high shear viscosity, or even the yield stress, of those suspensions [18–22]. Such particulate foams belong to the class of complex fluid foams and their rheology is expected to be understood from the intrinsic rheological behavior of the interstitial continuous material [23–31]. Larger particles or large aggregates of small particles can induce specific and interesting effects as soon as their size is comparable to the constrictions formed by the foam network. Criteria for capture of single particles or collective jamming of concentrated suspensions have been given in link with foam drainage properties [32–34]. Recent work has provided a consistent physical picture for the rheology of foams laden with hydrophilic particles [35–38].

In the following, we will focus on results involving solid spherical particles with radius  $a \gtrsim 1 \mu\text{m}$ . We will first review interfacial rheological studies for single armored fluid interfaces, as planar rafts and drops/bubbles (figure 1 - b-c-d). Second, we present recent work on rheology of granular films and gas marbles (figure 1 - a-e). Finally, we report on recent advances on the rheology of aqueous foams laden with hydrophilic grains (figure 1 g-h).

## I – Interfacial Rheology of Particulate Interface

Few works have recently reviewed the rheology of particle laden interfaces [39,40], from nano to microparticles at water/oil or water/air interfaces with various salt concentrations tuning the long range particles interactions. In the present review, we will focus on the specificities of micro-particles at water/air interfaces also called *granular rafts*.

### Modeling

Single liquid interfaces laden with hydrophobic particles are known to exhibit properties of both liquid interfaces and solid membranes. As for other complex interfaces [41], their interfacial rheological behaviors are described by the relation of the surface deformation to the surface stress. A general expression for the surface stress is given by:  $\sigma_s = \gamma I + \tau$  where  $\gamma$  is the interfacial or surface tension, which depends on particle surface fraction ( $\varphi$ ),  $I$  is the surface unit tensor and  $\tau$  is an extra stress. For a liquid-like viscous interface, following the Boussinesq-Scriven model, the extra stress  $\tau$  is a viscous stress  $\tau_v$  and writes [42]:  $\tau_v = [(\xi_s - \eta_s)\nabla_s \cdot v]I + 2\eta_s D_s$  where  $\xi_s$  is the surface (or interfacial) dilatational viscosity,  $\eta_s$  is the surface (or interfacial) shear viscosity,  $\nabla_s$  is the surface gradient operator,  $v$  is the surface velocity vector and  $D_s$  is the surface deformation rate tensor. For a solid-like elastic interface, following a linear elastic model [43], the extra stress  $\tau$  is an elastic stress  $\tau_e$  and writes:  $\tau_e = [(E_s - G_s)\nabla_s \cdot u]I + 2G_s U_s$  where  $E_s$  is the surface (or interfacial) dilatational modulus,  $G_s$  is the surface (or interfacial) shear modulus,  $u$  is the surface displacement vector and  $U_s$  the surface deformation tensor.

Finally, note that liquid-gas interface (simple interfaces laden with tensioactive molecules or complex interface laden with large “molecules” or particles) can exhibit elasticity if any change of the surface concentration changes its surface tension. In the case of an insoluble monolayer, which is usually the case for particles, this elasticity is characterized by the Gibbs modulus  $E_G = -A d\gamma/dA$  where  $A$  is the area of the interface.

Finally, as particle raft has a finite thickness  $t$  close to the particles size, a possible approach to characterize its mechanical behavior is to assimilate it to a thin elastic sheet with Young Modulus  $E_{3d}$  and Poisson coefficient  $\nu$  [44]. In such a case, the surface parameters are the following [45]: the stretching modulus  $E_s = E_{3d}t/2(1 - \nu)$ , the shear modulus  $G_s = E_{3d}t/2(1 + \nu)$  and the flexural (bending) rigidity  $B = E_{3d}t^3/12(1 - \nu^2)$ .

Dedicated instruments, apparatus and methods have been used to measure these properties for particles laden interfaces of constant or changing area. In the following we will present results obtained on Langmuir trough, pendant drop / rising bubble experiments, for which the surface area is compressed, and rheometrical shear flows experiments.

### *Particle rafts: Compression*

Since the pioneer work of Aveyard [46] for microparticles at water/oil interface, many authors [47,48] have used a Langmuir trough equipped with Wilhelmy plates to measure the surface tension ( $\gamma$ ) of monolayers whose surface area ( $A$ ) is varied by moving barriers while the quantity of particles is fixed. The surface pressure  $\Pi = \gamma_0 - \gamma$ , where  $\gamma_0$  is the surface tension of the particle-free interface, characterizes the resistance to compression of the monolayer. Typical behavior is reported on figure 2 – a where  $\Pi$  is plotted as a function of  $A$ . Along a compression experiment, from large to low surface areas, the observed behavior can be described as follows: at large surface area (low particle concentration) the surface pressure tends to zero; as the surface area decreases (the particle concentration increases), there is a first critical point ( $A^*$ ) for which the surface pressure increases steeply; then, there is a second critical point  $A_c$ , from which the surface pressure increases only slowly and tends to saturate, i.e.  $\Pi_c \approx \gamma_0 - \gamma_c$ . The change around  $A^*$  can be interpreted as a change of particle interaction from long range to short range [39], whereas the transition at  $A_c$  is associated to the buckling of the monolayer and thus to the liquid-like to solid-like transition. Cicuta et al. [48] showed that the pressure  $\Pi_c$  depends on the aspect ratio of the surface area ( $l/w =$  length between the moving barriers / width of the trough): at low aspect ratio  $\Pi_c \sim \gamma_0$ , then  $\Pi_c$  decays exponentially with  $l/w$ . Moreover, they measured a different surface pressure for Wilhelmy plate oriented parallel or orthogonal to the moving barriers. Using arguments based on the analogy with parietal friction observed in 3D granular silos, i.e Janssen effect [49], they were able to describe the exponential decay for the surface pressure. Recently, Saavedra et al. [50] have shown that the screening of the pressure stress within particle raft is even much stronger than expected.

For large compression (i.e.  $A < A_c$ ), particle rafts exhibit buckling characterized by wrinkling wavelength  $\lambda$ , as for thin elastic sheets. As shown by Vella et al. [44] this analogy allows to deduce the bulk (Young) modulus  $E_{3d}$  of the equivalent thin sheet:  $\lambda = \pi(16B/\rho g)^{1/4}$ . Their experimental results showed that  $E_{3d} \sim \gamma_0/a$  within the range of investigated particle sizes, i.e. from 2.5  $\mu\text{m}$  to 6 mm. Recently, Jambon-Puillet et al. [51] showed that the elastic description for granular raft compression is powerful to describe wrinkle wavelength, wrinkle-to-fold transition, and the fold shape at large compression, but it does not capture finer details such as secondary wave length and hysteretic behavior that are associated to solid friction. In the same trend, but in a dynamic regime, Planchette et al. [52] studied wave propagation along a particle raft. They measured the relation between celerity and wavelength for different particle diameters (within the range 30 to 160  $\mu\text{m}$ ) and contact angles  $\theta$ , and deduced the bending stiffness  $B$  by fitting their data according to the theory of thin elastic sheets [45]. They confirmed the scaling  $B = f(\theta) \times \gamma a^2$  [44,46,53] with  $f(\theta) = 2$  for  $\theta = \pi/2$  [46,53]. More recently, Petit et al. [54] explored the buckling of bidisperse particles rafts, and evidenced that the wavelength  $\lambda$  does not increase continuously with the

proportions  $\psi$  of large particles but rather exhibits a sharp transition. This result was explained by a percolation behavior with force chains supported only by the small particles.

### *Shrinkage of armored spherical bubbles and drops*

Xu et al. [55] and Monteux et al. [47] have studied the collapse of millimeter drops coated with micrometer-sized spherical PS particles, with particle-to-bubble size ratio  $a/R < 0.003$ . The drops were forced to shrink in size through progressive removal of their bulk liquid while their internal pressure  $\Delta P$  was measured. A typical result is presented in figure 2-b: below a given volume  $V_0$  (and a corresponding drop radius  $R_0$ ) the drop pressure deviates from the expected Laplace pressure  $2\gamma_0/R$  and instead decreases down to vanishing values. This transition was attributed to the strong particle interactions induced by the contraction of the interface during drop shrinkage. The pressure value at collapse was measured to be close to zero, which means that the mechanical equilibrium of the drop was maintained provided the applied (forcing) pressure was below  $\Delta P_{max}$  such that  $\Delta P_{max}/(2\gamma_0/R_0) \approx 0.8-0.9$ . This result can be understood as follows: Any bulk pressure reduction (with respect to the capillary pressure  $2\gamma_0/R_0$ ) induces an increase of the surface pressure  $\Pi$  within the monolayer [56]. Equivalently, the effective surface tension  $\gamma = (\gamma_0 - \Pi)$  decreases when the drop shrinks. When  $\gamma \approx 0$  there is strong compressive stress in the monolayer but the internal pressure is now too small to maintain the spherical shape, leading the destabilization (collapse) of the drop.

Later, Pitois et al. [57] have studied the collapse pressure of millimeter drops covered by monolayers of spherical PS particles, with  $a/R_0$  within the range 0.01-0.2. Whereas  $\Delta P_{max}/(2\gamma_0/R_0) \approx 0.9$  was measured for the smallest  $a/R$  values, in agreement with [47,55], the armor strength was found to increase significantly for  $a/R_0 > 0.1$ , which means that negative internal pressures can be reached in this regime (the free interface is negatively curved between the particles). Actually,  $\Delta P_{max}/(2\gamma_0/R_0) \approx 2$  for  $a/R_0 \approx 0.2$ , which means that the internal pressure reaches  $-2\gamma_0/R_0$  at collapse.

More recently, Taccoen et al. [58] have designed an experimental setup to study the behavior of armored bubbles (instead of drops, see figure 2-c). They reported that the collapse behavior of such bubbles is such that  $\Delta P_{max} \propto 1/R_0$ , independently of the particle size. It is to say that this result is fully consistent with previous results: within the range of investigated values for the particle-to-bubble size ratio, i.e.  $a/R_0 \leq 0.05$ , the reduced collapse pressure is almost constant (see figure 2-d). Therefore, the collapse behavior of armored bubbles is similar to the behavior described above for drops. Several studies have confirmed such a behavior, whatever the particle size, particle shape, i.e. dumbbell [59] and ellipsoidal [4] shapes, particle nature [4,59], or bubble/drop size. We stress that all the results from literature can be gathered on the same graph by plotting the reduced collapse pressure  $\Delta P_{max}/(2\gamma_0/R_0)$  (which is equivalent to  $\Pi_{max}/\gamma_0$ ) as a function of  $a/R_0$  (see figure 2-d). We show here that all the data can be described as follows:  $\Delta P_{max}/(2\gamma_0/R_0) \approx 0.8-1$  for  $a/R_0 \lesssim 0.1$ , which is similar to results obtained on Langmuir thought (i.e.  $\Pi_{max}/\gamma_0 \approx 1$ ), and  $\Delta P_{max}/(2\gamma_0/R_0) > 1$  for  $a/R_0 > 0.1$ .

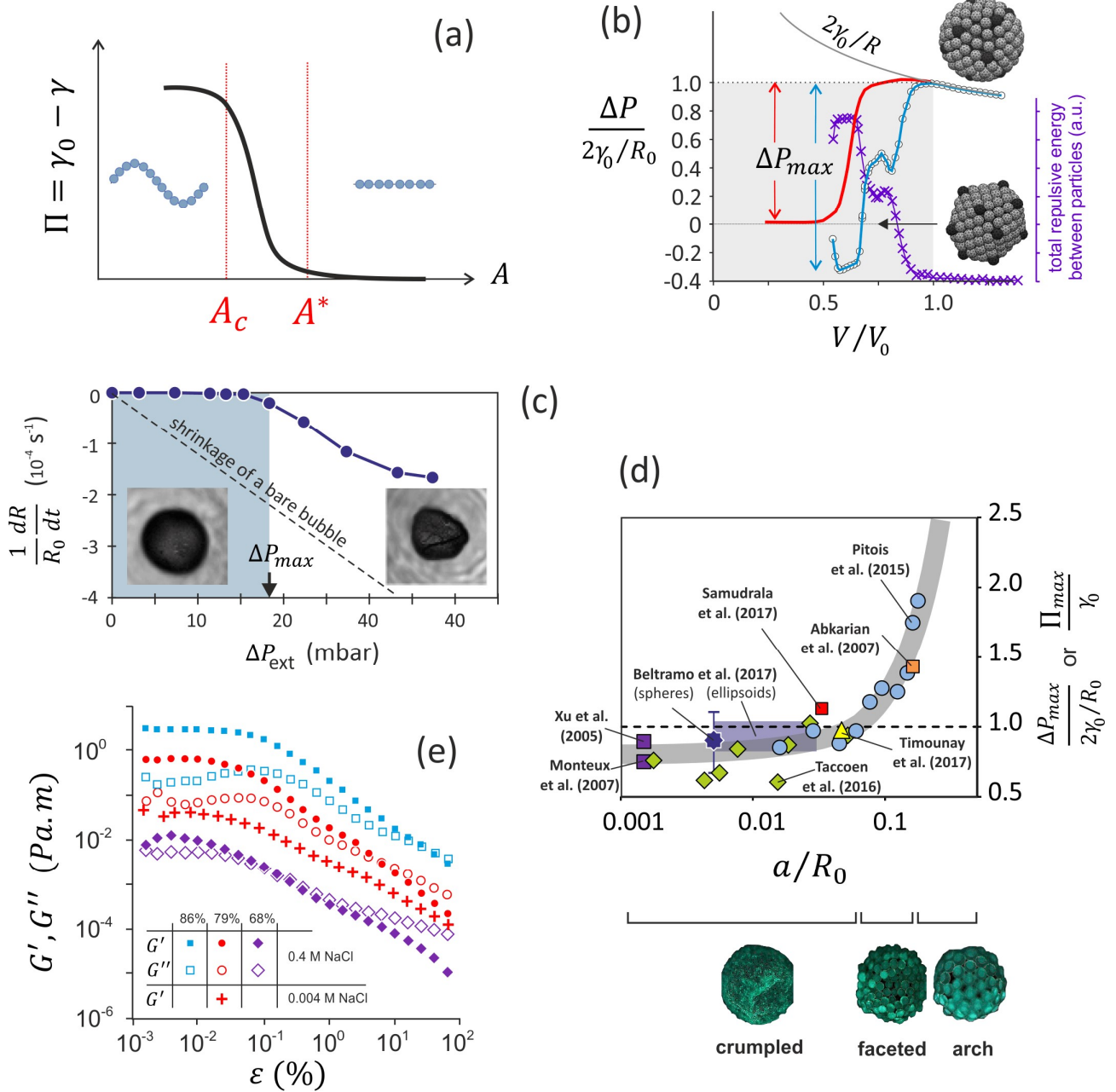


Figure 2: (a) sketch of surface pressure  $\Pi$  as a function the surface area ( $A$ ) of a particle monolayer. (b) Typical example for the evolution of internal pressure  $\Delta P$  of armored drops/bubbles as a function of their volume  $V$ . The effect of the armor can be observed when  $V$  is decreased below a reference value  $V_0$ , for which the corresponding capillary pressure is  $2\gamma_0/R_0$ . Red continuous line: experimental results for a drop covered with micrometer-sized PS particles (adapted from [47]). The particle-to-drop size ratio is about 0.003. Circles and crosses: Simulated internal pressure and repulsive energy between the particles for an armored bubble with particle-to-drop size ratio equal to 0.15 (adapted from [60]). The two pictures show the armored bubble at  $\Delta P / (2\gamma_0/R_0) \approx 1$  and 0 respectively. The collapse pressure  $\Delta P_{max}$  measures the pressure variation from the initial equilibrium state towards the irreversible collapse. (c) Shrinkage rate of an armored bubble as a function of the applied (forcing) pressure  $\Delta P_{ext}$  (adapted from [58]). This shows that there exists a pressure value  $\Delta P_{max}$  below which the bubble dissolution is arrested. The pictures show a stable bubble (left) and a collapsed bubble (right). (d) Reduced collapse pressure  $\Delta P_{max} / (2\gamma_0/R_0)$  (or equivalently the reduced surface pressure  $\Pi_{max} / \gamma_0$ ) as a function of the particle-to-bubble (or drop) size ratio  $a/R_0$ , for several results from literature (data of the referred-to articles have been used to calculate the presented parameters, and in some cases only average values are plotted for the sake of clarity). For data from Timounay et al., the presented reduced collapse pressure is  $\Delta P^- / (2\gamma^+ / R_0)$  (see the main text for more details). Images show armored drops at collapse for the three identified collapse regimes, i.e. crumpled, faceted and arch regimes. Each regime is associated to a range of collapse pressures and to the corresponding range of size ratio (adapted from [57]). (e) Viscoelastic shear moduli : storage  $G'$  (plain) and  $G''$  loss (hollow) for different particle surface concentrations and of salt concentrations, adapted from [61].

The observed behavior for the collapse pressure has been thought to result from the basic elasticity properties of the monolayer. Actually, the collapse of spherical shells is an old problem in elastic theory. It is known that the spherical shape is unstable for pressures larger than the critical pressure  $P_C = 4\sqrt{E_s B}/R_0^2$  [45]. For particle monolayers, we have  $E_s \sim \gamma_0$  and  $B \sim \gamma_0 a^2$ , so the critical pressure writes  $P_C \sim \gamma_0 a/R_0^2$ , and the reduced collapse pressure is therefore expected to be  $P_C/(2\gamma_0/R_0) \sim a/R_0$ . This behavior is not in agreement with experimental results presented in figure 2-d, which suggests that the classical model for elastic collapse should be adapted to the case of armored bubbles and drops. Dedicated physical models have been proposed to describe both the collapse pressure and the crumpled shape of the drop/bubble at collapse [56–58]. The basic idea is that as stress increases in the monolayer due to interface contraction, particles are pushed out of the plane by forces at contact, resulting in an accordion or a sinusoidal shape for the interface. In the same time capillary restoring forces restrain those motions and set the magnitude of the elastic modulus. Applying this approach Taccoen et al. [58] have derived an expression for the threshold pressure  $\Delta P_{max}$  above which mechanical stability is lost:  $\Delta P_{max}/(2\gamma_0/R_0) \cong 0.8$ . This value falls within the range of measured collapse pressures at small  $a/R_0$  values. Moreover, it has been suggested that out-of-plane motions are prevented for larger size ratios [57]. The underlying mechanism is the entanglement of particles through their contact network at the curved interface, leading to the formation of stable particle arches. This mechanism has been shown to modify the armor shape at collapse with respect to the crumpled shape observed for  $a/R_0 \ll 0.1$ : faceted shapes were observed for  $a/R_0 \approx 0.1$  [57,60] and spherical (i.e. undeformed until sudden collapse) shapes were observed for  $a/R_0 \approx 0.2$  [57].

The collapse of armor bubbles has been studied through numerical simulations performed by using the Surface Evolver software [60]. Due to the small number of particles that could be simulated, the study was focused on rather large particle-to-bubble size ratio, i.e.  $a/R_0 \approx 0.1-0.2$ . The authors were able to reproduce the so-called faceted regime described above, associated to negative internal pressures at collapse (see figure 2-b), or equivalently  $\Pi_{max}/\gamma_0 > 1$ . Note that the simulated collapse threshold is in agreement with measured collapse pressure in this regime [57]. Moreover, it was clearly shown that while the internal pressure decreases, the repulsive energy between particles increases (see figure 2-b), or equivalently the compressive stress increases in the monolayer.

#### *Particle rafts: Simple shear flow*

Different tools have been developed to characterize interfacial shear rheology for particle monolayers with fixed area and to measure the complex shear modulus  $G^* = G_s + i\omega\eta_s$ .

The magnetic rod rheometer [62,63] consists in imposing oscillatory shear to the interface between a fixed channel and a needle which is displaced by an electromagnetic force  $F$ . For microsized PS latex spheres forming aggregates at air/water interface due to salt addition in the subphase, Reynaert et al. [62] have estimated  $G^*$  from the force  $F$  and the needle displacement  $z$ :  $G^* = (F/z)((w - b)/(2L))$  where  $w$  and  $L$  are respectively the width and the length of the channel and  $b$  the radius of the needle. The shear modulus is deduced by assuming a simple superposition of the effect of the particle monolayer with the particle-free interface.

2D equivalents of classical 3D Couette geometries can be instrumented in standard rheometers using bicone or ring geometries. Their inherent sensitivity is lower than magnetic needle rheometers, but they enable usage of the wide range of experimental protocols and the choice between stress or strain control [64]. With this geometry, Barman et al. [61] have measured shear viscoelastic moduli for microsized PS spheres at the air-water for different aqueous salt

concentrations and particle surface concentrations. Similar experiments have been conducted with nanoparticles [65,66]. The linear interfacial rheological signature of  $G'$  and  $G''$  versus strain is characteristic of soft glassy material [67] (figure 2 - e): at low strain,  $G' \gg G''$  and  $G'$  and  $G''$  are expected to be constant for large enough particle surface fractions; for strain approaching a critical (yield) strain,  $G'$  decreases whereas  $G''$  increases slightly and  $G'$  and  $G''$  are of the same order of magnitude; at large strain,  $G'$  and  $G''$  both decrease and  $G' < G''$ . The magnitude of the shear modulus increases with the particle concentration [61,62] and with salt concentration [61]. The complex viscosity of the monolayer  $\eta_s = G^*(i\omega)$ , that may account for possible viscoelastic responses, is found also to increase with the particle concentration and to diverge when non-aggregated particles reach the packing surface fraction [62]. Note that as salt is added to the liquid phase, it induces aggregation of the charged particles [61,62,68] and thus changes the microstructure. Thanks to a careful study of the microstructure coupled with rheometry, Barman et al. showed that the magnitude of  $G^*$  is set locally by the degree of restricted particle motion (due to both interparticle attraction induced by capillarity and caging effect caused by local microstructure), but elasticity and yielding are rather linked to the mesostructural organization: large area of aligned particles along hexagonal packing is the signature of elastic interfaces; at large strains, a transition to viscous-like behavior is characterized by the breakup of these large domains into smaller domains that can move at the interface. Therefore, particle aggregation (which can be tuned by the chemistry of the solution) appears to be an efficient way to create complex interfacial systems with larger resistance to shear and to promote the stability of foams or emulsions. In addition, particle geometry and particle roughness [69] could be other parameters to be explored. For instance, ellipsoids increase the monolayer resistance to shear (larger  $G$  and  $\eta$  even at low particle coverage) [70].

## II - Rheology of Granular Films and Gas Marbles

Interpretation of rheometry experiments performed on armored air-water interface is nontrivial because bulk and interfacial flows have to be decoupled. Rheometry performed on particulate films is therefore of interest because it gets rid of the bulk/interfacial flow coupling and because it measures the mechanical properties of the elements present in foams [71,72].

The viscosity of free-standing particle laden films have been studied for particles within the *bridging* configuration [73] (see figs 1-a,bottom and 3-a). Retraction experiments of such granular films have been performed on rectangular frames: a mobile stick was placed on the rectangular frame, parallel to the short edge, and then the film was ruptured on one side, which induced the rapid motion of the stick. Local velocities were measured by PIV during the unstationary regime, i.e. right after the beginning of the retraction process (Fig 3-b). The equation for 2D momentum diffusion was solved by assuming inertial and viscous balance, and the comparison with the experimental velocity profiles has provided the 2D viscosity  $\mu_{2D}$  as a function of the particle surface fraction  $\varphi$ , as shown in figure 3-c. The 2D granular film behaves like a 2D suspension for which the viscosity diverges at the critical particle surface fraction equal to the random close packing, i.e.  $\varphi_c \approx 0.84$ . Actually, the experimental data can be described by models accounting for the viscous dissipation induced by individual particles motions in the liquid film. Similarly to 3D non-colloidal suspensions, the 2D dynamic viscosity follows a Krieger-Dougherty law [74]  $\mu_{2D} = \mu_{2D0}(1 - \varphi/\varphi_c)^{-k\varphi_c}$  with  $k \approx 1$  and  $\mu_{2D0} \approx 8 \cdot 10^{-5} Pa.s.m$  (figure 3c). At low  $\varphi$ ,  $\mu_{2D}$  tends to twice the interfacial dilatational viscosity of the liquid/air interfaces ( $\xi_s \approx 7 \cdot 10^{-5} Pa.s.m$ ), which is consistent with Trapeznikov's approximation [75] that states  $\mu_{2D0} = 2\xi_s + 2\eta_s + e\mu_{3D}$ , where the film thickness  $e \approx 40 \cdot 10^{-6} m$ , the bulk dynamical  $\mu_{3D} \approx 10^{-3} Pa.s$  and  $\eta_s \approx 10^{-6} Pa.s.m$ . Assuming that viscous energy is dissipated at the fluid interfaces around the particles, the model of

Mills and Snabre [76] adapted to our 2D geometry gives  $\mu_{2D} = \mu_{2D0} \varphi / (1 - \sqrt{\varphi/\varphi_c})$ , which is also consistent with the experimental data (figure 3-c).

Starting from the above-described particle film, a granular bubble (a so called *gas marble*) of radius  $R_0$  can be formed when the film detaches from the frame and closes over itself (see figure 3-d). These “hollow” objects were named in reference to the *liquid marbles*, but they appeared to be much stronger than their liquid counterpart [77]. The pressure of the bubble,  $P_{inner}$ , was measured to be equal to the pressure outside,  $P_{outer}$ , which means that the effective surface tension of the granular shell is equal to zero, as discussed above for armored drops. Their strength can be characterized as follows: By inflating or deflating the gas marble, Y. Timounay measured the maximal overpressure  $\Delta P^+ = \max(P_{inner} - P_{outer})$  that the bubble can resist without fracturing its granular shell and the minimal underpressure  $\Delta P^- = \min(P_{inner} - P_{outer})$  that the gas marble can resist without collapsing. In figure 3-d, the normalized extremal values for  $\Delta P^-/\Delta P_0$  and  $\Delta P^+/\Delta P_0$  are plotted as a function of the size ratio  $a/R_0$ , where  $\Delta P_0 = 4\gamma_0/R_0$  is the Laplace pressure of the corresponding particle-free bubbles with two interfaces. The gas marble can undergo both large overpressures and under-pressures, i.e. ten times larger than  $\Delta P_0$ . This behavior was attributed to the capillary-induced cohesion of the grains, which magnitude can be related to the mean radius of curvature  $r$  describing the liquid-gas interface within the monolayer pore space:  $\sigma_{cap} = \gamma_0/r$ . Such capillary stress provides exceptional cohesion properties for the gas marble’s shell, which can be described by an effective surface tension  $\gamma^+ \sim 10 \times \gamma_0$ , or equivalently  $\Delta P^+/\Delta P_0 \sim 10$ . Moreover, the resistance to collapse during deflation of gas marbles showed the existence of a high pressure threshold, i.e.  $|\Delta P^-| \sim 10 \times \Delta P_0$ . By analogy with the collapse behavior of elastic shells, the expected threshold is equal to  $16E(a/R_0)^2$ , which gives  $E \approx 20 \text{ kPa}$ , that is to say 100 times larger than the values reported for particles rafts [44,52] and classical armored drops [57]. On the other hand, a consistent link can be made with the collapse pressure of classical armored bubbles by considering that the reference pressure is  $4\gamma^+/R_0$  (i.e. instead of  $4\gamma_0/R_0$ ), providing a normalized collapse pressure  $\Delta P^-/(4\gamma^+/R_0) \approx 1$ , which falls within the expected range of values (see figure 2-e).

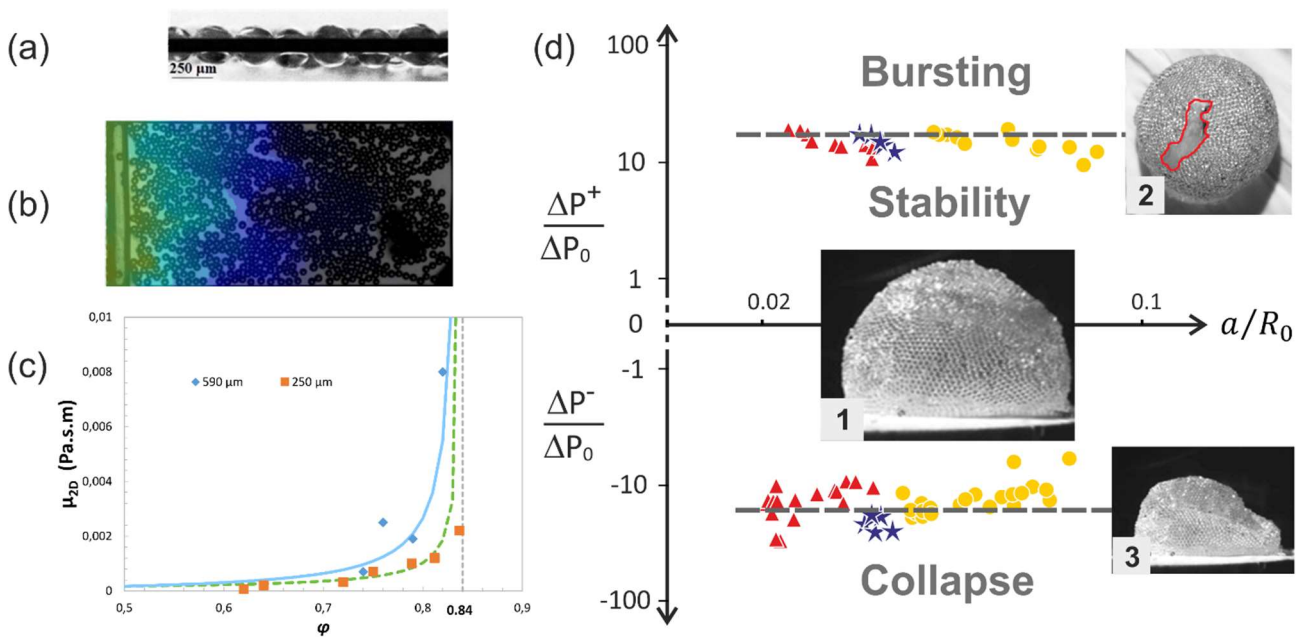


Figure 3: (a) profile view of granular film with particle of  $140\mu\text{m}$ , (b) top view of granular film where the mobile stick is on the left and move to the right, PIV images shows that velocities propagate through the film from left to right, (c) dynamic viscosities  $\mu_{2D}$  versus surface fraction of particles for two diameters ( $590\mu\text{m}$  and  $250\mu\text{m}$ ), the dotted curve corresponds to  $\mu_{2D} = \mu_{2D0} \phi / (1 - \sqrt{\phi/\phi_c})$  and Krieger-Dougherty law for  $k = 1$  corresponds to the solid curve, (d) Normalized critical overpressures ( $\Delta P^*/\Delta P_0$ ) and underpressures ( $\Delta P/\Delta P_0$ ) measured for gas marbles within both inflation and deflation conditions, respectively, as a function of bubble diameter  $D_b$ . Laplace pressure  $\Delta P_0 = 4\gamma/R_0$  is the pressure at equilibrium of the corresponding particle-free bubbles with two interfaces. The stability range of gas marbles is between the two horizontal dashed lines. The image n°1 is a side view of a gas marble within its stability range, the image 2 is a view of a gas marble after fracturing its granular shell, the image 3 is a view of a gas marble after collapsing.

### III – Rheology of Particle Foams

The rheology of foams loaded with hydrophilic particles has not been studied so far before the pioneer work of Cohen-Addad et al. [35]. Later, Gorlier et al. [36–38] have performed a series of experiments with well-controlled systems over a wide range for the particle-to-bubble size ratio, providing a global physical picture for the elasticity and the yield stress of such complex fluid foams.

#### Shear elastic modulus

Cohen-Addad et al. [35] have investigated the viscoelastic properties of foams made from a stable foam (Gillette shaving cream) and solid particles of average radius  $a$ , mainly glass and carbon beads, but also talc platelets. The particle-laden foams were obtained by whipping the Gillette foam and the particles. The bubble radius  $R$  was measured to be  $14\mu\text{m}$  and the reported particle-to-bubble size ratio  $a/R$  was within the range 0.3-5. Cone-plate or plate-plate cells were used to measure the complex shear modulus of foams laden with the different kinds of particles as a function of solid volume fractions  $\phi_p \lesssim 0.5$ . For low strain amplitudes, they observed a linear regime and predominantly elastic behavior characterized by an elastic modulus denoted  $G(\phi_p)$  which was found to increase drastically with  $\phi_p$ . The enhancement of  $G(\phi_p)$  is all the more pronounced that  $a/R$  is small. The authors analyzed their results in terms of *rigidity percolation threshold*: they assumed that the presence of capillary bridges, whose typical range is denoted  $2d$ , allows for the transmission of force necessary for rigidity percolation. According to the authors, the particle-laden foam could be compared to a dispersion of effective rigid elements of enhanced radius  $a + d$  that occupy a volume fraction  $\phi_p^{eff} = \phi_p(1 + d/R)^3$ . Under these conditions, the value for  $\phi_p$  at threshold, denoted  $\Phi_{pc}$ , is reached when a percolating cluster of effective rigid elements is formed, at volume fraction  $\Phi_{pc}^{eff}$ . In the limit of small particle volume fractions, the threshold  $\Phi_{pc}$  was determined by fitting the relation  $G(\phi_p)/G(0) \approx 1/(1 - \phi_p/\Phi_{pc})$  on the data, as shown in the inset of figure 4-f. Values obtained for  $\Phi_{pc}$  as a function of  $a/R$  are presented in figure 4-f, showing good agreement with predicted values assuming that  $\Phi_{pc}^{eff} \approx 0.42 \pm 0.04$  and  $h \approx 3.8 \pm 1.0\mu\text{m}$ , which was claimed to be within the expected range of capillary interactions.

Gorlier et al. [36,38] have studied the elastic behavior of foams produced with a dedicated in-line mixing method of precursor aqueous foam with polystyrene particle suspension. The foamy mixture was let to drain in the vane-cup rheometry cell before measurement of the shear elastic modulus within oscillatory conditions in the linear regime. Figure 4-d presents the results obtained for the reduced elastic modulus  $G(\phi_p)/G(0)$ , where  $G(0)$  is the elastic modulus estimated for the reference aqueous foam, i.e. the particle-free foam with same gas volume fraction  $\phi$  and same bubble size. The investigated range for the particle-to-bubble size ratio covered small values down to 0.01 which revealed that, for each  $\phi_p$  value,  $G(\phi_p)$  reaches an upper limit  $G_{max}(\phi_p)$  at small

$a/R$  values. It was also shown that for each  $\phi_p$  value,  $G(\phi_p)$  reaches a lower limit  $G_{min}(\phi_p)$  at large  $a/R$  values. This behavior could be interpreted in terms of a threshold  $\Phi_{pc}$ , as shown in figure 4-f. However, a natural description for the effect of  $a/R$  was proposed as a transition for the elastic modulus  $G(\phi_p)$  between the two limits  $G_{max}(\phi_p)$  and  $G_{min}(\phi_p)$ , which physical meaning has been clarified as follows.

The strong enhancement observed for  $G_{max}(\phi_p)$  has been attributed to the intrinsic elasticity of the interstitial skeleton made of packed particles, which has been proved to form only for small  $a/R$  values (see figure 4-a). The elastic contribution of the solid foam-shaped skeleton was assumed to superimpose to that of the bubble assembly  $G(0)$ . According to this approach, the elastic modulus of the bulk granular packing, which forms the skeleton, was expected to be at least two orders of magnitude larger than  $G(0)$ . This was confirmed by rheometry experiments performed on the bulk granular packing [38], and the authors showed that the small pressure  $P_{conf}$  exerted by the foam bubbles on the confined granular packing is responsible for this effect. For  $G_{min}(\phi_p)$ , it was recognized that in the regime of large  $a/R$  values, isolated large particles are embedded in the elastic foam medium (Figure 4-c) and the corresponding strengthening effect has been deduced from previous work on solid particles embedded in continuous matrix [78]. This approach showed full agreement with the data (see figure 4-d).

In order to highlight the transition behavior between  $G_{max}(\phi_p)$  and  $G_{min}(\phi_p)$  over the whole range of particle volume fractions, a normalized elastic modulus has been introduced:  $\tilde{G} = (G - G_{min}) / (G_{max} - G_{min})$ , which measures the magnitude of  $G(\phi_p)$  with respect to both upper and lower bounds, for which  $\tilde{G} = 1$  and  $\tilde{G} = 0$  respectively. It has been shown that, for all  $\phi_p$  values,  $\tilde{G}$  decreases from 1 over two orders of magnitude as  $a/R$  increases from 0.01 to 1, following a power law behavior:  $\tilde{G} \sim (a/R)^{-1.5}$ . An example for such a behavior is shown in figure 4-g, where data from Cohen-Addad et al. [35] have been successfully included within this description. Note that the decrease is not observed from the smallest  $a/R$  values, for which  $\tilde{G} \approx 1$ . This behavior has been attributed to the fact that particles can pack between bubbles until their size become larger than the size of interstices between bubbles, then further increase of  $a/R$  results in the progressive exclusion of the particles from the bulk foam network (Figure 4-b-c). This transition appeared to be better described by the so-called confinement parameter  $\lambda$ , which has been introduced initially to predict the capture of single particles within the foam network [34], and which has been proved to be a control parameter for the drainage of particle-laden foams [79–81]. Finally, it has been shown that the normalized parameter  $\tilde{G}$  follows the same behavior than the counterpart normalized parameters for drainage and mechanics of particle-laden foams [81,82].

### *Yield stress*

As far as we know, the issue of how the yield stress of aqueous foams is modified by solid hydrophilic particles has been considered only in the paper from Gorlier et al. [37]. Yield stress  $\tau_y(\phi_p)$  was measured from start-flow curves at low shear rates for the systems presented above. The reduced shear stress  $\tau_y(\phi_p) / \tau_y(0)$  was measured to increase as a function of both  $\phi_p$  and the inverse of the particle size. The authors have analyzed their results with the same basic idea than for the elastic modulus: the yield stress of particle-laden foams exhibits a transition behavior between two limit values, i.e.  $\tau_{y,max}(\phi_p)$  for small  $a/R$  values and  $\tau_{y,min}(\phi_p)$  for large  $a/R$  values.

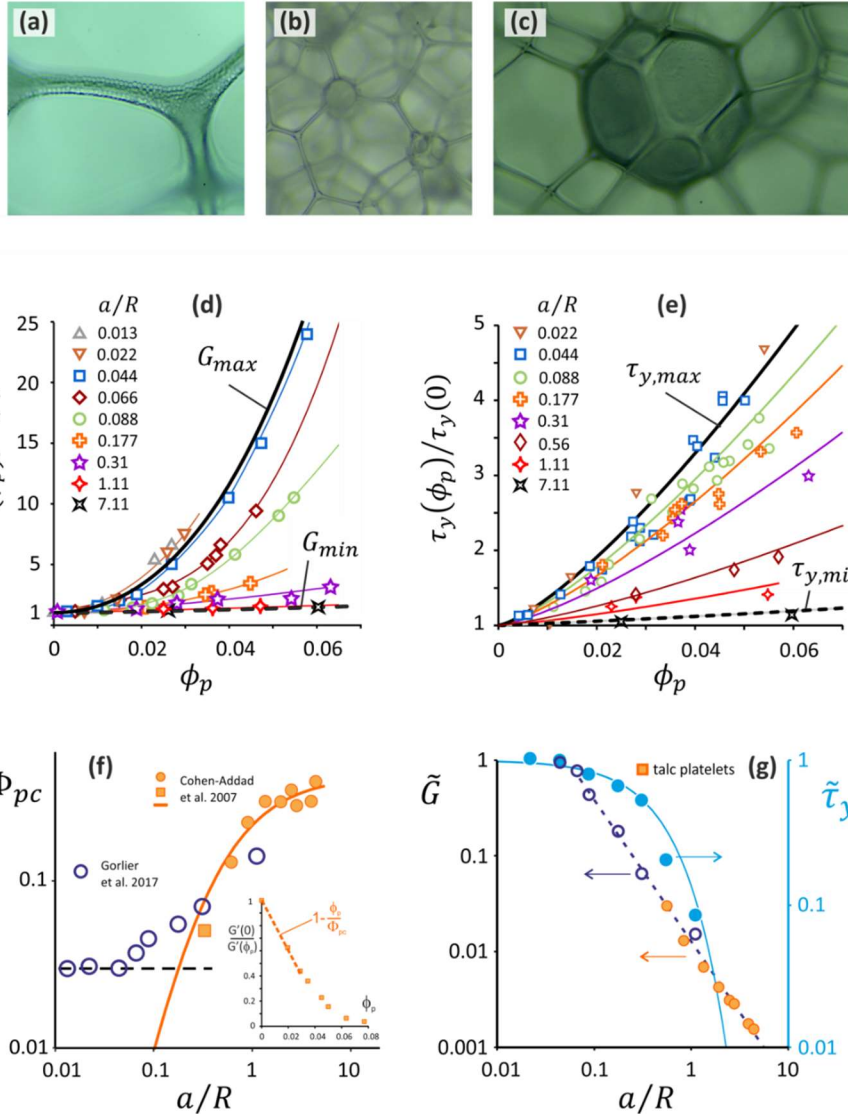


Figure 4: (a,b,c) Images from [37] showing solid spheres configuration in aqueous foam with bubble radius  $R = 225 \mu\text{m}$ . Particle radius  $a = 10 \mu\text{m}$  (a),  $70 \mu\text{m}$  (b) and  $250 \mu\text{m}$  (c). (d) Elastic modulus  $G(\phi_p)$  of particle-laden foam, divided by the elastic modulus  $G(0)$  of the reference particle-free foam ( $R = 225 \mu\text{m}$ ), as a function of the particle volume fraction  $\phi_p$  for several values of the particle-to-bubble size ratio  $a/R$  [36]. Solid curves indicated by  $G_{min}$  and  $G_{max}$  correspond respectively to regimes for large and small  $a/R$  values (see main text for details). (e) Yield stress  $\tau_y(\phi_p)$  of particle-laden foam, divided by the yield stress  $\tau_y(0)$  of the reference particle-free foam ( $R = 225 \mu\text{m}$ ), as a function of the particle volume fraction  $\phi_p$  for several values of the particle-to-bubble size ratio  $a/R$  [37]. Solid curves indicated by  $\tau_{y,min}$  and  $\tau_{y,max}$  correspond respectively to regimes for large and small  $a/R$  values (see main text for details). (f) Rigidity percolation threshold  $\Phi_{pc}$  as proposed in [35] as a function of the particle-to-bubble size ratio  $a/R$  ( $\phi_p = 0.07$ ). Data from [35] (circles represent spherical particles and the square represents talc particles) and [36] are presented together, showing the existence of a lower limit for  $\Phi_{pc}$  at small  $a/R$  values (indicated by the dotted line). The solid line corresponds to  $\Phi_{pc} = \Phi_{pc}^{eff} (1 + d/R)^{-3}$  with parameters  $\Phi_{pc}^{eff} = 0.42$  and  $d = 3.8 \mu\text{m}$  [35]. Inset: Illustration of how the parameter  $\Phi_{pc}$  is determined from the plot of the inverse of the reduced elastic modulus as a function of the particle volume fraction, by fitting the equation  $G(0)/G(\phi_p) \approx 1 - \phi_p/\Phi_{pc}$ . (g) Normalized elastic modulus  $\tilde{G}$  [36] ( $\phi_p = 0.07$ ) and normalized yield stress  $\tilde{\tau}_y$  [37] ( $\phi_p = 0.05$ ) (see main text for more details) as a function of the particle-to-bubble size ratio  $a/R$ . Data from [35] are also presented (circles represent spherical particles and the square represents talc particles). The dashed line corresponds to  $\tilde{G} \sim (a/R)^{-1.5}$  and the solid line corresponds to  $\tilde{\tau}_y \approx \exp(-2a/R)$ .

In the regime of large particles embedded in aqueous foam, micro-mechanical approach suggests that the yield stress can be deduced from the knowledge of the elastic modulus [83–85]. Applying this result to particle-laden foam gave the following relation:  $\tau_{y,min}(\phi_p)/\tau_y(0) =$

$\left((1 - \phi_p) G_{min}(\phi_p)/G(0)\right)^{1/2}$ , which was found to describe accurately the yield stress in this regime (see figure 4-e). On the other hand, the yield stress in the regime of small  $a/R$  values is much more difficult to describe because it involves the shear-induced rupture of the granular packing confined between the bubbles. Rupture of bulk granular solids is known to be described by the Mohr-Coulomb criterion, where the shear stress at rupture is proportional to the confinement pressure:  $T_y = \mu P_{conf}$ , where  $\mu$  is the so-called internal friction coefficient. By resorting to yield stress measurements with foams made with calibrated yield stress fluids [37], the authors were able to propose a simple relation to describe the yield stress of particle-laden foams in the regime of small  $a/R$  values (see figure 4-e):  $\tau_{y,max}(\phi_p)/\tau_y(0) = 1 + c\phi_p^{4/3}Ca_y^{2/3}$ , where  $c \approx 200$  is a numerical coefficient and  $Ca_y = T_y R/\gamma$  is the Bingham capillary number. This relation means that the foam's yield stress is governed by the Mohr-Coulomb condition for the interstitial granular skeleton.

The transition regime was considered similarly to the case of the elastic modulus and the normalized yield stress was introduced:  $\tilde{\tau}_y = (\tau_y - \tau_{y,min})/(\tau_{y,max} - \tau_{y,min})$ . In contrast to  $\tilde{G}$ ,  $\tilde{\tau}_y$  was not found to follow a power law behavior, but instead it follows an exponential decay (see figure 4-e), i.e.  $\tilde{\tau}_y \approx \exp(-2a/R)$ . Such a difference has been attributed to bubble rearrangement involved by yielding (i.e. the so-called T1 topological events [86]), which can be significantly prevented by particles if the average distance between neighboring particles is less than one bubble size. Actually, bubbles bridging neighboring particles possess yielding properties which are related to the Rayleigh-Plateau instability [87], which contrasts with yielding of bulk foam bubbles.

## Conclusion

Results presented in this review highlight the different ways solid particles can be used to influence the rheological behavior of films and foams. Small hydrophobic particles can adsorb to the liquid-gas interfaces and form the so-called armored interfaces and Pickering foams. Whereas long-term stability against both coalescence and ripening seems to be the strong feature of Pickering foams, applied shear has a catastrophic impact on their stability, and their rheological behavior has not been studied so far. On the other hand, studies performed on the rheology of the armored interfaces, either particle rafts, either particle films or armored bubbles, allow those stability issues to be understood.

Shear modulus magnitude of "loose" particle raft increases with average particle surface fraction and is set locally by the degree of restricted particle motion, but yielding are rather linked to the mesostructural organization. Approaching the random close packing of the particles in 2D, the transition to jamming is observed by the divergence of the viscosity for both particle raft and granular film. A "dense" particle raft compression can be modeled by continuum theory of thin elastic sheet whose moduli are particle size dependent for monodisperse raft, but the granular character has to be accounted for confined geometry or for bidisperse systems due to wall friction and granular chain forces.

Studies on shrinkage of single armored bubbles are consistent with those performed on particle rafts. Moreover, they give significant understanding on how attached particle layers can oppose the capillary-driven foam ripening process if they are within the jammed regime. This property, which can be quantified by the bubble collapse pressure, appears to be significantly

influenced by the particle-to-bubble size ratio. At large particle-to-bubble size ratio, the pressure collapse can overpass the reference Laplace pressure of the bubble due to entanglement of particles at the curved interface, leading to the formation of stable particle arches and the faceting of the shell, instead of crumpling observed at collapse for small size ratio. For bubbles armored by a granular film, i.e. Gas Marbles, the collapse pressure is one order of magnitude larger than for classical armored bubbles due to the capillary cohesion between the particles that support the bubble liquid film.

For hydrophilic particle laden foams, the elasticity and yielding under shear are strongly dependent of the particle-to-bubble size ratio as well as the particle volume fraction. The smallest particles organize through the network between the gas bubbles and form a granular skeleton. Such a structure with tightly packed particles is responsible for the strongly enhanced elasticity observed in this particle-to-bubble size regime. Moreover, yielding is governed by the classical Mohr-Coulomb criterion. For large particle-to-bubble size ratio, the particles are excluded from the bulk foam network, and the rheological properties of the foam are only weakly enhanced.

## Acknowledgments

We thank E. Lorenceau, X. Chateau, Y. Khidas and Y. Timounay for fruitful discussions.

## References :

- [1] W. Ramsden, Separation of Solids in the Surface-Layers of Solutions and “Suspensions” (Observations on Surface-Membranes, Bubbles, Emulsions, and Mechanical Coagulation). -- Preliminary Account, Proc. R. Soc. London. 72 (1903) 156–164. doi:10.1098/rspl.1903.0034.
- [2] S.U. Pickering, CXCVI. - Emulsions, J. Chem. Soc. Trans. 91 (1907) 2001–2021. doi:10.1039/CT9079102001.
- [3] U.T. Gonzenbach, A.R. Studart, E. Tervoort, L.J. Gauckler, Stabilization of foams with inorganic colloidal particles, Langmuir. (2006). doi:10.1021/la061825a.
- \*[4] P.J. Beltramo, M. Gupta, A. Aliche, I. Liascukiene, D.Z. Gunes, C.N. Baroud, J. Vermant, Arresting dissolution by interfacial rheology design, Proc. Natl. Acad. Sci. (2017) 201705181. doi:10.1073/pnas.1705181114.
- [5] E. Rio, W. Drenckhan, A. Salonen, D. Langevin, Unusually stable liquid foams, Adv. Colloid Interface Sci. (2014). doi:10.1016/j.cis.2013.10.023.
- [6] B.P. Binks, R. Murakami, Phase inversion of particle-stabilized materials from foams to dry water, Nat. Mater. (2006). doi:10.1038/nmat1757.
- [7] G. Kaptay, On the equation of the maximum capillary pressure induced by solid particles to stabilize emulsions and foams and on the emulsion stability diagrams, Colloids Surfaces A Physicochem. Eng. Asp. (2006). doi:10.1016/j.colsurfa.2005.12.021.
- [8] T.S. Horozov, B.P. Binks, Particle-stabilized emulsions: A bilayer or a bridging monolayer?, Angew. Chemie - Int. Ed. (2006). doi:10.1002/anie.200503131.
- [9] T.S. Horozov, Foams and foam films stabilised by solid particles, Curr. Opin. Colloid Interface Sci. (2008). doi:10.1016/j.cocis.2007.11.009.
- [10] Y. Timounay, E. Lorenceau, F. Rouyer, Opening and retraction of particulate soap films, EPL. (2015). doi:10.1209/0295-5075/111/26001.
- \*[11] A. Maestro, E. Rio, W. Drenckhan, D. Langevin, A. Salonen, Foams stabilised by mixtures of nanoparticles and oppositely charged surfactants: relationship between bubble shrinkage and foam coarsening, Soft Matter. 10 (2014) 6975–6983. doi:10.1039/C4SM00047A.
- [12] S. Arditty, V. Schmitt, F. Lequeux, Interfacial properties in solid-stabilized emulsions, Eur. Phys. J. B. 44 (2005) 381–393. doi:10.1140/epjb/e2005-00137-0.
- [13] B. Wolf, S. Lam, M. Kirkland, W.J. Frith, Shear thickening of an emulsion stabilized with

- hydrophilic silica particles, *J. Rheol.* (N. Y. N. Y). 51 (2007) 465. doi:10.1122/1.2714642.
- [14] W.J. Frith, M. Kirkland, R. Pichot, B. Wolf, Formation, Stability, and Rheology of Particle Stabilized Emulsions: Influence of Multivalent Cations, *Ind. Eng. Chem. Res.* 47 (2008) 6434–6444. doi:10.1021/ie071629e.
- [15] G.N. Sethumadhavan, A.D. Nikolov, D.T. Wasan, Stability of Liquid Films Containing Monodisperse Colloidal Particles., *J. Colloid Interf. Sci.* 240 (2001) 105–112. doi:10.1006/jcis.2001.7628.
- [16] S.K. Bindal, G. Sethumadhavan, a. D. Nikolov, D.T. Wasan, Foaming mechanisms in surfactant free particle suspensions, *AIChE J.* 48 (2002) 2307–2314. doi:10.1002/aic.690481020.
- [17] R.. Kao, D.. Edwards, D.. Wasan, E. Chen, Measurement of interfacial dilatational viscosity at high rates of interface expansion using the maximum bubble pressure method. I. Gas—liquid surface, *J. Colloid Interface Sci.* 148 (1992) 247–256. doi:10.1016/0021-9797(92)90133-7.
- [18] A.M. Sani, K.K. Mohanty, Incorporation of clay nano-particles in aqueous foams, *Colloids Surfaces A Physicochem. Eng. Asp.* 340 (2009) 174–181. doi:10.1016/j.colsurfa.2009.03.026.
- [19] R. Guillermic, A. Salonen, J. Emile, A. Saint-Jalmes, Surfactant foams doped with laponite: unusual behaviors induced by aging and confinement, *Soft Matter.* 5 (2009) 4975–4982. doi:10.1039/b914923f.
- [20] A. Britan, M. Liverts, G. Ben-Dor, S.A. Koehler, N. Bennani, The effect of fine particles on the drainage and coarsening of foam, *Colloids Surfaces A Physicochem. Eng. Asp.* 344 (2009) 15–23. doi:10.1016/j.colsurfa.2009.03.011.
- [21] F. Carn, A. Colin, O. Pitois, M. Vignes-Adler, R. Backov, Foam drainage in the presence of nanoparticle-surfactant mixtures., *Langmuir.* 25 (2009) 7847–7856. doi:10.1021/la900414q.
- [22] F. Carn, A. Colin, O. Pitois, R. Backov, Foam drainage study during plateau border mineralisation, *Soft Matter.* 8 (2012) 61–65. doi:10.1039/c1sm06778h.
- [23] J. Goyon, F. Bertrand, O. Pitois, G. Ovarlez, Shear induced drainage in foamy yield-stress fluids, *Phys. Rev. Lett.* 104 (2010). doi:10.1103/PhysRevLett.104.128301.
- [24] M. Kogan, L. Ducloué, J. Goyon, X. Chateau, O. Pitois, G. Ovarlez, Mixtures of foam and paste: Suspensions of bubbles in yield stress fluids, *Rheol. Acta.* 52 (2013). doi:10.1007/s00397-013-0677-7.
- [25] L. Ducloué, O. Pitois, J. Goyon, X. Chateau, G. Ovarlez, Rheological behaviour of suspensions of bubbles in yield stress fluids, *J. Nonnewton. Fluid Mech.* 215 (2015) 31–39. doi:10.1016/j.jnnfm.2014.10.003.
- [26] L. Ducloué, O. Pitois, L. Tocquer, J. Goyon, G. Ovarlez, Yielding and flow of foamed metakaolin pastes, *Colloids Surfaces A Physicochem. Eng. Asp.* 513 (2017). doi:10.1016/j.colsurfa.2016.11.015.
- [27] L. Ducloué, O. Pitois, J. Goyon, X. Chateau, G. Ovarlez, Coupling of elasticity to capillarity in soft aerated materials., *Soft Matter.* 10 (2014) 5093–8. doi:10.1039/c4sm00200h.
- [28] I. Lesov, S. Tcholakova, N. Denkov, Drying of particle-loaded foams for production of porous materials: mechanism and theoretical modeling, *RSC Adv.* 4 (2014) 811–823. doi:10.1039/c3ra44500c.
- [29] I. Lesov, S. Tcholakova, N. Denkov, Factors controlling the formation and stability of foams used as precursors of porous materials., *J. Colloid Interface Sci.* 426 (2014) 9–21. doi:10.1016/j.jcis.2014.03.067.
- [30] A. Salonen, R. Lhermerout, E. Rio, D. Langevin, A. Saint-Jalmes, Dual gas and oil dispersions in water: Production and stability of foamulsion, *Soft Matter.* 8 (2012) 699–706. doi:10.1039/c1sm06537h.
- [31] F. Gorlier, Y. Khidas, O. Pitois, Coupled elasticity in soft solid foams, *J. Colloid Interface Sci.* 501 (2017). doi:10.1016/j.jcis.2017.04.033.
- [32] B. Haffner, Y. Khidas, O. Pitois, Flow and jamming of granular suspensions in foams., *Soft*

- Matter. 10 (2014) 3277–3283. doi:10.1039/c4sm00049h.
- [33] B. Haffner, Y. Khidas, O. Pitois, The drainage of foamy granular suspensions, *J. Colloid Interface Sci.* 458 (2015) 200–208. doi:10.1016/j.jcis.2015.07.051.
- [34] N. Louvet, R. Höhler, O. Pitois, Capture of particles in soft porous media, *Phys. Rev. E.* 82 (2010) 041405.
- \*[35] S. Cohen-Addad, M. Krzan, R. Höhler, B. Herzhaft, Rigidity percolation in particle-laden foams, *Phys. Rev. Lett.* 99 (2007) 168001. doi:10.1103/PhysRevLett.99.168001.
- \*\*[36] F. Gorlier, Y. Khidas, O. Pitois, Elasticity of particle-loaded liquid foams, *Soft Matter.* 13 (2017) 4533–4540. doi:10.1039/c7sm00679a.
- \*\*[37] F. Gorlier, Y. Khidas, O. Pitois, Yielding of complex liquid foams, *J. Rheol. (N. Y. N. Y.)*. 61 (2017) 919–930. doi:10.1122/1.4994786.
- [38] F. Gorlier, Y. Khidas, A. Fall, O. Pitois, Optimal strengthening of particle-loaded liquid foams, *Phys. Rev. E - Stat. Nonlinear, Soft Matter Phys.* 95 (2017) 042604. doi:10.1103/PhysRevE.95.042604.
- [39] J.H.J. Thijssen, J. Vermant, Interfacial rheology of model particles at liquid interfaces and its relation to (bicontinuous) Pickering emulsions, *J. Phys. Condens. Matter.* (2018). doi:10.1088/1361-648X/aa9c74.
- [40] A. Maestro, E. Santini, D. Zabiegaj, S. Llamas, F. Ravera, L. Liggieri, F. Ortega, R.G. Rubio, E. Guzman, Particle and particle-surfactant mixtures at fluid interfaces: Assembly, morphology, and rheological description, *Adv. Condens. Matter Phys.* (2015). doi:10.1155/2015/917516.
- [41] N. Jaensson, J. Vermant, Tensiometry and rheology of complex interfaces, *Curr. Opin. Colloid Interface Sci.* (2018). doi:10.1016/j.cocis.2018.09.005.
- [42] L.E. Scriven, Dynamics of a fluid interface Equation of motion for Newtonian surface fluids, *Chem. Eng. Sci.* (1960). doi:10.1016/0009-2509(60)87003-0.
- [43] T. Verwijlen, L. Imperiali, J. Vermant, Separating viscoelastic and compressibility contributions in pressure-area isotherm measurements, *Adv. Colloid Interface Sci.* (2014). doi:10.1016/j.cis.2013.09.005.
- \*\*[44] D. Vella, P. Aussillous, L. Mahadevan, Elasticity of an interfacial particle raft, *Europhys. Lett.* (2004). doi:10.1209/epl/i2004-10202-x.
- [45] L.D. Landau, E.M. Lifshitz, J.B. Sykes, W.H. Reid, E.H. Dill, *Course of Theoretical Physics - Theory of Elasticity*, 1960. doi:10.1063/1.3057037.
- [46] R. Aveyard, J.H. Clint, D. Nees, N. Quirke, Structure and collapse of particle monolayers under lateral pressure at the octane/aqueous surfactant solution interface, *Langmuir.* (2000). doi:10.1021/la000060i.
- \*[47] C. Monteux, J. Kirkwood, H. Xu, E. Jung, G.G. Fuller, Determining the mechanical response of particle-laden fluid interfaces using surface pressure isotherms and bulk pressure measurements of droplets, *Phys. Chem. Chem. Phys.* 9 (2007) 6344–6350. doi:10.1039/b708962g.
- \*[48] P. Cicuta, D. Vella, Granular character of particle rafts, *Phys. Rev. Lett.* (2009). doi:10.1103/PhysRevLett.102.138302.
- [49] H.A. Janssen, Versuche über getreidedruck in Silozellen, *Zeitschrift Des Vereins Dtsch. Ingenieure.* (1895). doi:citeulike-article-id:11888572.
- [50] O. Saavedra V., H. Elettro, F. Melo, Progressive friction mobilization and enhanced Janssen's screening in confined granular rafts, *Phys. Rev. Mater.* 2 (2018) 43603. doi:10.1103/PhysRevMaterials.2.043603.
- [51] E. Jambon-Puillet, C. Josserand, S. Protière, Wrinkles, folds, and plasticity in granular rafts, *Phys. Rev. Mater.* 1 (2017) 42601. doi:10.1103/PhysRevMaterials.1.042601.
- [52] C. Planchette, E. Lorenceau, A.L. Biance, Surface wave on a particle raft, *Soft Matter.* (2012). doi:10.1039/c2sm06859a.
- [53] P.A. Kralchevsky, K. Nagayama, Capillary interactions between particles bound to interfaces, liquid films and biomembranes, *Adv. Colloid Interface Sci.* (2000). doi:10.1016/S0001-

8686(99)00016-0.

- \*[54] P. Petit, A.L. Biance, E. Lorenceau, C. Planchette, Bending modulus of bidisperse particle rafts: Local and collective contributions, *Phys. Rev. E.* (2016). doi:10.1103/PhysRevE.93.042802.
- [55] H. Xu, S. Melle, K. Golemanov, G. Fuller, Shape and buckling transitions in solid-stabilized drops, *Langmuir.* 21 (2005) 10016–10020. doi:10.1021/la0507378.
- [56] S. Kam, W. Rossen, Anomalous Capillary Pressure, Stress, and Stability of Solids-Coated Bubbles., *J. Colloid Interface Sci.* 213 (1999) 329–339. doi:10.1006/jcis.1999.6107.
- [57] O. Pitois, M. Buisson, X. Chateau, On the collapse pressure of armored bubbles and drops, *Eur. Phys. J. E.* (2015). doi:10.1140/epje/i2015-15048-9.
- [58] N. Taccoen, F. Lequeux, D.Z. Gunes, C.N. Baroud, Probing the mechanical strength of an armored bubble and its implication to particle-stabilized foams, *Phys. Rev. X.* 6 (2016). doi:10.1103/PhysRevX.6.011010.
- [59] N. Samudrala, J. Nam, R. Sarfati, R.W. Style, E.R. Dufresne, Mechanical stability of particle-stabilized droplets under micropipette aspiration, *Phys. Rev. E.* 95 (2017) 012805. doi:10.1103/PhysRevE.95.012805.
- \*\*[60] M. Abkarian, A.B. Subramaniam, S.H. Kim, R.J. Larsen, S.M. Yang, H. a. Stone, Dissolution arrest and stability of particle-covered bubbles, *Phys. Rev. Lett.* 99 (2007) 3–6. doi:10.1103/PhysRevLett.99.188301.
- \*\*[61] S. Barman, G.F. Christopher, Role of capillarity and microstructure on interfacial viscoelasticity of particle laden interfaces, *J. Rheol. (N. Y. N. Y.)*. (2016). doi:10.1122/1.4935128.
- [62] S. Reynaert, P. Moldenaers, J. Vermant, Interfacial rheology of stable and weakly aggregated two-dimensional suspensions, *Phys. Chem. Chem. Phys.* (2007). doi:10.1039/b710825g.
- [63] S. Reynaert, C.F. Brooks, P. Moldenaers, J. Vermant, G.G. Fuller, Analysis of the magnetic rod interfacial stress rheometer, *J. Rheol. (N. Y. N. Y.)*. (2008). doi:10.1122/1.2798238.
- [64] P. Erni, P. Fischer, E.J. Windhab, V. Kusnezov, H. Stettin, J. Lauger, Stress- and strain-controlled measurements of interfacial shear viscosity and viscoelasticity at liquid/liquid and gas/liquid interfaces, *Rev. Sci. Instrum.* (2003). doi:10.1063/1.1614433.
- [65] D.Y. Zang, E. Rio, D. Langevin, B. Wei, B.P. Binks, Viscoelastic properties of silica nanoparticle monolayers at the air-water interface, *Eur. Phys. J. E.* (2010). doi:10.1140/epje/i2010-10565-7.
- [66] D.Y. Zang, E. Rio, G. Delon, D. Langevin, B. Wei, B.P. Binks, Influence of the contact angle of silica nanoparticles at the air-water interface on the mechanical properties of the layers composed of these particles, *Mol. Phys.* (2011). doi:10.1080/00268976.2010.542778.
- [67] P. Sollich, Rheological constitutive equation for a model of soft glassy materials, *Phys. Rev. E - Stat. Physics, Plasmas, Fluids, Relat. Interdiscip. Top.* (1998). doi:10.1103/PhysRevE.58.738.
- [68] P. V. Petkov, K.D. Danov, P.A. Kralchevsky, Monolayers of charged particles in a Langmuir trough: Could particle aggregation increase the surface pressure?, *J. Colloid Interface Sci.* (2016). doi:10.1016/j.jcis.2015.09.075.
- [69] H.J. Wilson, R.H. Davis, Shear stress of a monolayer of rough spheres, *J. Fluid Mech.* (2002). doi:10.1017/S0022112001006838.
- [70] B. Madivala, J. Fransaer, J. Vermant, Self-assembly and rheology of ellipsoidal particles at interfaces, *Langmuir.* (2009). doi:10.1021/la803554u.
- [71] F. Bouchama, J.M. Di Meglio, Two-dimensional rheology of soap films, *J. Phys. Condens. Matter.* (1996). doi:10.1088/0953-8984/8/47/056.
- [72] F. Bouchama, J.M. Di Meglio, Rheological studies of freely suspended soap films, *Colloid Polym. Sci.* (2000). doi:10.1007/s003960050032.
- [73] Y. Timounay, F. Rouyer, Viscosity of particulate soap films: Approaching the jamming of 2D capillary suspensions, *Soft Matter.* 13 (2017). doi:10.1039/c7sm00090a.
- [74] I.M. Krieger, T.J. Dougherty, A Mechanism for Non-Newtonian Flow in Suspensions of

- Rigid Spheres, *Trans. Soc. Rheol.* (1959). doi:10.1122/1.548848.
- [75] A.A. Trapeznikov, Application of the method of two-dimensional viscosity and shear strength to the investigation of the structure and composition of two-sided films and surface layers in solutions of soaps and saponins, *Proc. 2nd Int. Congr. Surf. Act.* (1957) 242–258. <http://scitation.aip.org/content/aip/magazine/physicstoday/article/66/12/10.1063/PT.3.2212>.
- [76] P. Mills, P. Snabre, Apparent viscosity and particle pressure of a concentrated suspension of non-Brownian hard spheres near the jamming transition, *Eur. Phys. J. E.* (2009). doi:10.1140/epje/i2009-10530-7.
- \*\*[77] Y. Timounay, O. Pitois, F. Rouyer, Gas Marbles: Much Stronger than Liquid Marbles, *Phys. Rev. Lett.* 118 (2017). doi:10.1103/PhysRevLett.118.228001.
- [78] F. Mahaut, F. Bertrand, P. Coussot, X. Chateau, G. Ovarlez, Suspensions of noncolloidal particles in yield stress fluids: Experimental and micromechanical approaches, *AIP Conf. Proc.* 1027 (2008) 671–673. doi:10.1063/1.2964804.
- [79] Y. Khidas, B. Haffner, O. Pitois, Capture-induced transition in foamy suspensions., *Soft Matter.* 10 (2014) 4137–4141. doi:10.1039/c4sm00246f.
- [80] B. Haffner, Y. Khidas, O. Pitois, B. Haffner, Y. Khidas, O.P. Flow, J.G. Sus-, Flow and Jamming of Granular Suspensions in Foams, *Soft Matter.* (2014). doi:10.1039/c4sm00049h.
- [81] B. Haffner, Y. Khidas, O. Pitois, The drainage of foamy granular suspensions, *J. Colloid Interface Sci.* 458 (2015) 200–208. doi:10.1016/j.jcis.2015.07.051.
- [82] Y. Khidas, B. Haffner, O. Pitois, Critical size effect of particles reinforcing foamed composite materials, *Compos. Sci. Technol.* 119 (2015) 62–67. doi:10.1016/j.compscitech.2015.09.024.
- [83] X. Chateau, G. Ovarlez, K.L. Trung, Homogenization approach to the behavior of suspensions of noncolloidal particles in yield stress fluids, *J. Rheol. (N. Y. N. Y.)*. 52 (2008) 489–506. doi:10.1122/1.2838254.
- [84] F. Mahaut, S. Mokéddem, X. Chateau, N. Roussel, G. Ovarlez, Effect of coarse particle volume fraction on the yield stress and thixotropy of cementitious materials, *Cem. Concr. Res.* 38 (2008) 1276–1285. doi:10.1016/j.cemconres.2008.06.001.
- [85] F. Mahaut, X. Chateau, P. Coussot, G. Ovarlez, Yield stress and elastic modulus of suspensions of noncolloidal particles in yield stress fluids, *J. Rheol. (N. Y. N. Y.)*. 52 (2008) 287. doi:10.1122/1.2798234.
- [86] I. Cantat, S. Cohen-Addad, F. Elias, F. Graner, R. Höhler, O. Pitois, F. Rouyer, *Foams: Structure and Dynamics*, Oxford University Press, Oxford, 2013.
- [87] S.J. Cox, D. Weaire, M. Fatima Vaz, The transition from three-dimensional to two-dimensional foam structures, *Eur. Phys. J. E.* 7 (2002) 311–315. doi:10.1140/epje/i2011-11082-y.